

Experimental 4-intensity decoy-state quantum key distribution with asymmetric basis detector efficiency

Hui Liu^{1,2}, Zong-Wen Yu^{3,4}, Mi Zou^{1,2}, Yan-Lin Tang⁷, Yong Zhao⁷,
Jun Zhang^{1,2}, Xiang-Bin Wang^{3,5,6,*}, Teng-Yun Chen^{1,2,†}, Jian-Wei Pan^{1,2‡}

¹*Hefei National Laboratory for Physical Sciences at Microscale and Department of Modern Physics,*

University of Science and Technology of China, Hefei, Anhui 230026, China

²*CAS Center for Excellence in Quantum Information and Quantum Physics,*

University of Science and Technology of China, Hefei, Anhui 230026, China

³*State Key Laboratory of Low Dimensional Quantum Physics,*

Department of Physics, Tsinghua University,

Beijing 100084, People's Republic of China

⁴*Data Communication Science and Technology Research Institute,*

Beijing 100191, People's Republic of China

⁵*Jinan Institute of Quantum Technology, SAICT,*

Jinan 250101, People's Republic of China

⁶*Department of Physics, Southern University of Science and Technology,*

Shenzhen, 518055, People's Republic of China

⁷*QuantumCTek Corporation Limited, Hefei, Anhui 230088, China*

The decoy-state method has been developed rapidly in quantum key distribution (QKD) since it is immune to photon-number splitting attacks. However, two basis detector efficiency asymmetry, which exists in realistic scenarios, has been ignored in the prior results. By using the recent 4-intensity decoy-state optimization protocol, we report the first implementation of high-rate QKD with asymmetric basis detector efficiency, demonstrating 1.9 to 33.2 times higher key rate than previous protocols in the situation of large basis detector efficiency asymmetry. The results ruled out an implicitly assumption in QKD that the efficiency of Z basis and X basis are restricted to be same. This work pave the way towards a more practical QKD setting.

* Email Address: xbwang@mail.tsinghua.edu.cn

† Email Address: tychen@ustc.edu.cn

‡ Email Address: pan@ustc.edu.cn

INTRODUCTION

Quantum key distribution (QKD) has continuously been focused since the first protocol proposed by Bennett and Brassard in 1984¹. However, the unconditionally security of the ideal BB84 has been frustrated by a lot of realistic imperfections, one prominent of which is the lack of the practical single photon source. It is more feasible for Alice to utilize the attenuated laser, i.e., the weak coherent pulses (WCP) as signal states, which results in a loophole for the photon-number splitting (PNS) attack^{2,3}. Fortunately, based on the original idea by Hwang⁴, the decoy-state method^{5,6} appeared in time. It has dramatically improve the performance of QKD with the attenuated laser by providing better bounds on the gain and the error rate of single photon states. In the past decade, noteworthy theoretical improvements have been proposed to continuously improve the performance of decoy-state QKD⁷⁻¹⁰. Experiments either over optical fiber or free-space have advanced significantly in the meantime¹¹⁻²⁰. Specially, QKD has been demonstrated at a transmission distance up to 7600 km in free-space²⁰ and more than 400 km in optical fiber^{16,19}.

Nevertheless, the practical applications of QKD combined with the one-time pad scheme are still pinned by low secure key rate. In addition, an implicit assumption for detector model in the existed results is that the efficiencies of Z basis and X basis are almost the same. It seems like a simple assumption but does not always meet realistic scenarios. For instance, it could be resulted from the efficiency asymmetry of single photon detectors in the passive basis choice protocol, or the imperfection during measurment bases switching in the active basis choice protocol. A common approach is reducing higher efficiency to balance detector efficiency asymmetry at the price of introducing additional losses.

Here, by making simple modifications to a commercial QKD system, we implement a novel 4-intensity decoy-state QKD protocol using biased bases²¹, which can provide higher key rate than previous traditional 3-intensity protocols with unbiased bases, especially in a large degree of basis detector efficiency asymmetry. Setting the detector efficiency asymmetry of two bases $\eta_Z/\eta_X = 2$ and 10 respectively, we change channel distance over different lengths of standard telecom fiber up to 150 km and demonstrate as much as 1.9 to 33.2 times higher key rate than previous protocols. These results have moved QKD towards a more practical setting.

THEORY

In the novel 4-intensity QKD protocol²¹, Alice prepares two different coherent sources in the Z basis with intensities μ_{Z_1} and μ_{Z_2} ; and two different coherent sources in the X basis with intensities μ_{X_1} and μ_{X_2} , with probabilities $p_{\alpha_j}(\alpha = Z, X; j = 1, 2)$ respectively. Without losing the generality, we assume $\mu_{\alpha_1} < \mu_{\alpha_2}(\alpha = Z, X)$. The coherent state whose phase is selected uniformly at random can be regarded as a mixture of photon number states, i.e., $\rho_{\alpha_j} = \sum_k a_{k,\alpha_j} |k\rangle\langle k|$ with $a_{k,\alpha_j} = e^{-\mu_{\alpha_j}} \mu_{\alpha_j}^k / k!$ for $\alpha = Z, X$ and $j = 1, 2$. In the protocol, Bob measures the received pulses in the Z and X bases with probabilities q^Z and q^X respectively. After the preparation and measurement of N_t pulses, Alice and Bob obtain the observable $N_{\alpha_j}^\omega$ and $M_{\alpha_j}^\omega$ which are the number of successful counts and error counts when Alice sends the pulses from source α_j and Bob measures them in the ω basis. Here α and ω can take both Z and X . We also denote $S_{\alpha_j}^\omega$ and $T_{\alpha_j}^\omega$ as the yield and error yield, respectively, with $S_{\alpha_j}^\omega = N_{\alpha_j}^\omega / (p_{\alpha_j} q^\omega N_t)$ and $T_{\alpha_j}^\omega = M_{\alpha_j}^\omega / (p_{\alpha_j} q^\omega N_t)$.

In Ref.²¹, a delicate point has been put forward that even in the asymptotic case, i.e., $s_0^Z \neq s_0^X$ and $s_{1,\alpha_1}^Z \neq s_{1,\alpha_2}^X$. Here s_{k,α_j}^ω is the yield of k -photon pulses prepared from source α_j and measured in the ω basis. The reason $s_{1,Z}^Z \neq s_{1,X}^X$ is simply due to the asymmetry of detection efficiencies and dark counts in different bases. Such asymmetry can come from either imperfect control of two of the devices inside Labs, or Eve's attack. In order to take a better treatment, the decoy-state method jointly in different bases has been studied²¹. For this goal, the observed number of counts of pulses prepared in one basis but measured in another basis shall be used. In particular, it is assumed that $s_{1,Z}^Z = s_{1,X}^Z$ and $s_{1,Z}^X = s_{1,X}^X$ are valid. Given these equations, one does not have to study the decoy-state method completely separately in each basis.

In all real experiment, the total number of pulses sent by Alice is finite. In order to extract the secret final key, we have to consider the effect of statistical fluctuations caused by the finite size. In this case, yields of the same state out of different sources are not always rigorously equal to each other, i.e., $s_{k,\alpha_1}^\omega \neq s_{k,\alpha_2}^\omega$. Accordingly²¹, with the observed values $S_{\alpha_j}^\omega$, one can lower bound the mean value $\langle s_{1,\alpha}^\omega \rangle$ for a given value of $\langle s_0^\omega \rangle$ with the following equations

$$\langle s_{1,\alpha}^\omega \rangle \geq \langle s_1^{\omega,L} \rangle = \max_{\alpha=Z,X} [\langle s_{1,\alpha}^{\omega,L} \rangle (\langle s_0^\omega \rangle)], \quad (1)$$

and

$$\langle s_{1,\alpha}^{\omega,L} \rangle (\langle s_0^\omega \rangle) = \frac{1}{A_{\alpha_1\alpha_2}^{1,2}} [a_{2,\alpha_2} \underline{S}_{\alpha_1}^\omega - a_{2,\alpha_1} \overline{S}_{\alpha_2}^\omega - A_{\alpha_1\alpha_2}^{0,2} \langle s_0^\omega \rangle], \quad (2)$$

where $A_{\alpha_1\alpha_2}^{0,2} = a_{0,\alpha_1} a_{2,\alpha_2} - a_{0,\alpha_2} a_{2,\alpha_1}$, $A_{\alpha_1\alpha_2}^{1,2} = a_{1,\alpha_1} a_{2,\alpha_2} - a_{1,\alpha_2} a_{2,\alpha_1}$, and $\underline{S}_{\alpha_j}^\omega = S_{\alpha_j}^\omega / (1 + \delta_{\alpha_j}^\omega)$, $\overline{S}_{\alpha_j}^\omega = S_{\alpha_j}^\omega / (1 - \delta_{\alpha_j}^\omega)$. By using the multiplicative form of the Chernoff bound, with a fixed failure probability ϵ , we can give an interval of $\langle S_{\alpha_j}^\omega \rangle$ with the observable $S_{\alpha_j}^\omega$, $[\underline{S}_{\alpha_j}^\omega, \overline{S}_{\alpha_j}^\omega]$, which can bound the value of $\langle S_{\alpha_j}^\omega \rangle$ with a probability of at least $1 - \epsilon$. Explicitly, we have $\delta_{\alpha_j}^\omega = \delta(N_{\alpha_j}^\omega S_{\alpha_j}^\omega, \epsilon)$ with the function $\delta(x, y) = [-\ln(y/2) + \sqrt{(\ln(y/2))^2 - 8 \ln(y/2)x}] / (2x)$. With the mean values $\langle s_1^{\omega,L} \rangle$ defined in Eq.(1), the lower bounds of $s_{1,\alpha_2}^\alpha (\alpha = Z, X)$ can be calculated with

$$s_{1,\alpha_2}^{\alpha,L} = \langle s_1^{\alpha,L} \rangle (1 - \delta_{1,\alpha_2}), \quad (3)$$

where $\delta_{1,\alpha_2} = \delta(N_{1,\alpha_2}^\alpha \langle s_1^{\alpha,L} \rangle, \epsilon)$. Here and after, we define $N_{k,\alpha_j}^\omega = a_{k,\alpha_j} p_{\alpha_j} q^\omega N_t$ as the number of k -photon pulses prepared in source α_j and measured in the basis ω .

Second, we can also formulate the phase-flip error rate of single-photon states. Explicitly, we have

$$e_{1,Z}^{ph} = e_{1,X_1}^X \leq e_{1,X_1}^{X,U} = \frac{\overline{T}_{X_1}^X - a_{0,X_1} \langle s_0^X \rangle (1 - \delta_{0,X_1}^X) / 2}{a_{1,X_1} s_{1,X_1}^{X,L}}, \quad (4)$$

where $\delta_{0,X_1}^X = \delta(N_{0,X_1}^X \langle s_0^X \rangle, \epsilon)$. In a finite-key-size case, we can apply the large data size approximation of the random sampling method to upper bound the phase error rate $e_1^{p,Z}$ of single-photon pulses prepared and measured in the Z basis with the failure probability ϵ

$$e_1^{p,Z} \leq e_1^{p,Z,U} = e_{1,X_1}^{X,U} + \theta_Z^X, \quad (5)$$

where $\theta_Z^X = \sqrt{n_\theta / d_\theta}$ with $d_\theta = \frac{(1-g_X)g_X \ln 2}{2(1-e_1)e_1}$, $n_\theta = -\log[\epsilon \sqrt{e_1(1-e_1)n_X n_Z / (n_X + n_Z)}] / (n_X + n_Z)$, and $g_X = \frac{n_X}{n_X + n_Z}$. Here we write $n_X = N_{1,X_1}^X$, $n_Z = N_{1,Z_2}^Z$ and $e_1 = e_{1,X_1}^{X,U}$ for simplicity. Note that $e_1^{p,Z,U}$ is a function of $\langle s_0^X \rangle$. Straightly, we can also formulate the upper bound of the phase-flip error rate of single-photon counts in the X basis, being denoted by $e_1^{p,X,U}$. We omit the explicit formula here since it is just trivially written analogically to Eq.(5).

Note that $\langle s_0^X \rangle$ (or $\langle s_0^Z \rangle$) is the common variable in both quantities $s_{1,X_2}^{X,L}$ and $e_1^{p,Z,U}$ (or quantities $s_{1,Z_2}^{Z,L}$ and $e_1^{p,X,U}$) shown in Eq.(3) and Eq.(5) respectively. We need to know the range of them for the final key rate calculation. In the 4-intensity protocol without the

assumption of vacuum, we can lower bound $\langle s_0^\omega \rangle$ by

$$\langle s_0^\omega \rangle \geq \langle s_0^{\omega,L} \rangle = \max_{\alpha=X,Z} \{ \langle s_0^{\omega,L} \rangle(\alpha), 0 \}, \quad (6)$$

where

$$\langle s_0^\omega \rangle \geq \langle s_0^{\omega,L} \rangle(\alpha) = \frac{a_{1,\alpha_2} \underline{S}_{\alpha_1}^\omega - a_{1,\alpha_1} \overline{S}_{\alpha_2}^\omega}{A_{\alpha_1\alpha_2}^{0,1}}, \quad (7)$$

and $A_{\alpha_1\alpha_2}^{0,1} = a_{0,\alpha_1} a_{1,\alpha_2} - a_{0,\alpha_2} a_{1,\alpha_1}$. By simply attributing all the errors to the vacuum pulses, we can upper bound of $\langle s_0^X \rangle$ with

$$\langle s_0^\omega \rangle \leq \langle s_0^{\omega,U} \rangle = \min \{ 2\overline{T}_{\omega_1}^\omega / a_{0,\omega_1}, \overline{S}_{Z_1}^\omega / a_{0,Z_1}, \overline{S}_{X_1}^\omega / a_{0,X_1} \}. \quad (8)$$

With these preparations, the final key rate of the 4-intensity protocol can be calculated with the following worst-case estimation

$$R = \min_{\langle s_0^Z \rangle, \langle s_0^X \rangle} [\mathcal{R}(\langle s_0^Z \rangle, \langle s_0^X \rangle)] \quad (9)$$

over the region for all possible values of $\langle s_0^Z \rangle$ and $\langle s_0^X \rangle$ in $[\langle s_0^{Z,L} \rangle, \langle s_0^{Z,U} \rangle]$ and $[\langle s_0^{X,L} \rangle, \langle s_0^{X,U} \rangle]$, respectively. Here

$$\mathcal{R}(\langle s_0^Z \rangle, \langle s_0^X \rangle) = \mathcal{R}_Z(\langle s_0^Z \rangle, \langle s_0^X \rangle) + \mathcal{R}_X(\langle s_0^Z \rangle, \langle s_0^X \rangle), \quad (10)$$

and

$$\mathcal{R}_\alpha(\langle s_0^Z \rangle, \langle s_0^X \rangle) = p_{\alpha_2} q^\alpha \{ a_{1,\alpha_2} s_{1,\alpha_2}^{\alpha,L} [1 - H(e_1^{p,\alpha,U})] - f S_{\alpha_2}^\alpha H(E_{\alpha_2}^\alpha) \}, \quad (11)$$

for $\alpha = Z, X$. Here f is the efficiency factor of the error-correction method used, $H(x) = -x \log_2(x) - (1-x) \log_2(1-x)$ is the binary Shannon entropy function. Note that in such a case we need to calculate the final key rate with two variables $\langle s_0^Z \rangle$ and $\langle s_0^X \rangle$ jointly.

EXPERIMENT

The polarization encoding is implemented in our experiment. FIG.1 illustrates the scheme of our experimental setup. The Z and X basis consists of $\{|H\rangle, |V\rangle\}$ and $\{|+\rangle, |-\rangle\}$, respectively, as four states for the standard BB84 protocol. The signals are generated at a system

clock rate of 625 MHz by 8 DFB lasers, half of which are used for generating signal state and the rest are used for decoy state. Alice encodes her qubits in Z or X basis in accordance with random bit values generated beforehand. The pulse width is about 100 ps and its wavelength center is at 1550.12 nm. These pulses are naturally phase randomized due to direct modulation onto DFB lasers. Utilizing 8 manual attenuators after each DFB laser, Alice realizes the intensity ratio of two intensities in each basis approximately. None of the DFB laser generated the pulse when vacuum pulse are need. Four PMBSs, two PMPBSs and a SMBS server for guiding pulses from different diodes to one optical fiber. The optical pulse intensity is strongly attenuated to single-photon level via an EVOA.

A 10 GHz FBG is inserted at Alice for three reasons. First, it guarantees that the spectrum of 8 DFB lasers are overlapped in a narrow range to get rid of the loopholes exploiting the pulses wavelength discrepancies. The second issue is that it achieves fine adjustment of the state intensities coordinated with the precise temperature control of the DFB laser. At last, it reduces the chromatic dispersion effects in long single-mode optical fiber. A suitable Dispersion Compensating Fiber is installed to compensate dispersion effects further and compress the pulses width, which guarantees that the pulse width is smaller than the detector effective gate width after long distance propagation.

The synchronization pulses are generated by a 1570 nm DFB laser operating at 100 kHz. In order to synchronize the entire experimental systems and reduce optical fiber costs, the synchronization pulses emitted from Alice are multiplexed with signal pulses by a 100 G DWDM and transmitted through the same single-mode optical fiber to Bob. A SOA is utilized to amplify the intensity of synchronization pulses to guarantee that Bob's PD receive sufficient optical power. A DWDM inserted before his PD is typically introduced filter undesired noise from the SOA.

Naively, Bob passively selects the measurement basis by a 1×2 SMBS with the splitting ratio of q_X . It indicates that the received photons are measured either on the X or Z basis randomly with probabilities of q_X and $q_Z = 1 - q_X$, respectively. Cooled to -50°C , four InGaAs APDs operating in gated Geiger mode are used to detect signals at 1.25 GHz gating frequency. The effective gating window width is 180 ps and the dead time is 500 ps, which is an optimal trade-off between the detection efficiency and the after pulses rate. The detection efficiency is about 10% at a dark count probability of 2.50×10^{-7} per gate. For convenience, we inserted two 3 dB or even 10 dB attenuations, one before each of two APDs for X basis, to

get a larger efficiency asymmetry and demonstrate the effectiveness of difference protocols. We thus regard the attenuations as a part of the APDs.

Alice and Bob have to develop a stable polarization reference frame initially owing to the polarization mode dispersion (PMD) effects in long distance single-mode optical fiber. Bob applies corresponding DC voltage on a pair of EPCs to align Alice's polarization states to the polarizing axes of the PBSs inserted before the APDs. The optical misalignment error rate e_d is around 1.5%. Note that the optical misalignment error rate of Z and X basis are independent. The polarization can remain stable for more than 20 minutes, which is long enough for our experiment.

RESULTS

Using same system parameters in Table I to perform a numerical optimization for consistency and taking the effects of statistical fluctuations into account, we implement three decoy-state BB84 protocols: (I) traditional 3-intensity protocol⁷ with basis detector efficiency symmetry, where Bob reduce higher detector efficiency to balance asymmetry $\eta_Z = \eta_X$; (II) 3-intensity protocol with basis detector efficiencies asymmetry²¹, where in both bases, Alice select the same intensities and proportions, and Bob measures the received pulses with the same probabilities, that is, $q_Z = q_X = 50\%$; (III) 4-intensity protocol²¹, where $q_Z \neq q_X$. In all protocols, the signal pulses μ_{Z_2} and μ_{X_2} are used for key generation, while other intensity pulses are used as decoy states to estimate the amount of privacy amplification necessary. The extra insertion loss in Bob is about 2.5-2.7 dB due to different BSs in different protocols. Thanks to the high clock rate, sufficient signal pulses are send by Alice during an uninterrupted session lasting 16.16 s to calculate the final key rate. We repeat the experiment 30 times and calculate the average and variance of the final key rate, which is shown in FIG.2. Details of the main implementation parameters and results are shown in the Supplemental Material.

In the first experiment, we set the detector efficiency of the InGaAs APD $\eta_Z = 10\%$ and $\eta_X = 5\%$, that is, the asymmetry $\eta_Z/\eta_X = 2$, and change the distance between Alice and Bob from 87 km to 150 km. The results are shown in FIG.2 (a). Consequently, 4-intensity protocol dramatically gives measurable advantage over two types of 3-intensity protocol. For example, 4-intensity protocol obtain a key rate of 39 kbps in 87 km, which is 3.0 times

that of 3-intensity protocol and 4.8 times that of 3-intensity protocol with basis detector efficiencies symmetry. And 4-intensity yield a secret key rate of 36.7 bps in a maximal distance of 150 km. In contrast, not even a bit of secure key can be extracted with both two types of 3-intensity. In the second experiment, we increase the mismatch on purpose and set $\eta_Z = 10\%$ and $\eta_X = 1\%$. FIG. 2(b) presents the experiment results. The experiment data of the 87 km case is used as an example to demonstrate the improvement of 4-intensity protocol. 4-intensity protocol obtain a key rate of 20 kbps in 87 km, which is 3.6 times that of 3-intensity protocol and 33.2 times that of 3-intensity protocol with basis detector efficiencies symmetry.

CONCLUSION

In summary, we have demonstrated, for the first time, an implementation of decoy-state QKD system with asymmetric basis detector efficiencies by the recent 4-intensity decoy-state optimization protocol. The secure key rate is higher than previous traditional 3-intensity protocols with unbiased bases results by 1.9 to 33.2 times. Besides, our results ruled out an implicitly assumption in QKD that the efficiency of Z basis and X basis are restricted to be same. Therefore, the implementation is an excellent candidate for future quantum key distribution.

ACKNOWLEDGMENTS

This work was supported by the National Key R&D Program of China (2017YFA0303903), the National Natural Science Foundation of China (Grant No. 61875182), and Anhui Initiative in Quantum Information Technologies and Fundamental Research Funds for the Central Universities (WK2340000083).

-
1. Bennett, C. H. & Brassard, G. Proceedings of the ieee international conference on computers, systems and signal processing (1984).
 2. Brassard, G., Lütkenhaus, N., Mor, T. & Sanders, B. C. Limitations on practical quantum cryptography. *Physical Review Letters* **85**, 1330 (2000).

3. Lütkenhaus, N. Security against individual attacks for realistic quantum key distribution. *Physical Review A* **61**, 052304 (2000).
4. Hwang, W.-Y. Quantum key distribution with high loss: toward global secure communication. *Physical Review Letters* **91**, 057901 (2003).
5. Wang, X.-B. Beating the photon-number-splitting attack in practical quantum cryptography. *Physical review letters* **94**, 230503 (2005).
6. Lo, H.-K., Ma, X. & Chen, K. Decoy state quantum key distribution. *Physical review letters* **94**, 230504 (2005).
7. Wang, X.-B., Hiroshima, T., Tomita, A. & Hayashi, M. Quantum information with gaussian states. *Physics reports* **448**, 1–111 (2007).
8. Hayashi, M. Upper bounds of eavesdroppers performances in finite-length code with the decoy method. *Physical Review A* **76**, 012329 (2007).
9. Jiang, H., Gao, M., Yan, B., Wang, W. & Ma, Z. Universally-composable finite-key analysis for efficient four-intensity decoy-state quantum key distribution. *The European Physical Journal D* **70**, 78 (2016).
10. Chau, H. Decoy-state quantum key distribution with more than three types of photon intensity pulses. *Physical Review A* **97**, 040301 (2018).
11. Rosenberg, D. *et al.* Long-distance decoy-state quantum key distribution in optical fiber. *Physical review letters* **98**, 010503 (2007).
12. Schmitt-Manderbach, T. *et al.* Experimental demonstration of free-space decoy-state quantum key distribution over 144 km. *Physical Review Letters* **98**, 010504 (2007).
13. Yuan, Z., Sharpe, A. & Shields, A. Unconditionally secure one-way quantum key distribution using decoy pulses. *Applied physics letters* **90**, 011118 (2007).
14. Chen, T.-Y. *et al.* Field test of a practical secure communication network with decoy-state quantum cryptography. *Optics express* **17**, 6540–6549 (2009).
15. Liu, Y. *et al.* Decoy-state quantum key distribution with polarized photons over 200 km. *Optics express* **18**, 8587–8594 (2010).
16. Boaron, A. *et al.* Secure quantum key distribution over 421 km of optical fiber. *Physical review letters* **121**, 190502 (2018).
17. Liao, S.-K. *et al.* Satellite-to-ground quantum key distribution. *Nature* **549**, 43 (2017).

18. Peng, C.-Z. *et al.* Experimental long-distance decoy-state quantum key distribution based on polarization encoding. *Physical review letters* **98**, 010505 (2007).
19. Yin, H.-L. *et al.* Measurement-device-independent quantum key distribution over a 404 km optical fiber. *Physical review letters* **117**, 190501 (2016).
20. Liao, S.-K. *et al.* Satellite-relayed intercontinental quantum network. *Physical review letters* **120**, 030501 (2018).
21. Yu, Z.-W., Zhou, Y.-H. & Wang, X.-B. Reexamination of decoy-state quantum key distribution with biased bases. *Physical Review A* **93**, 032307 (2016).

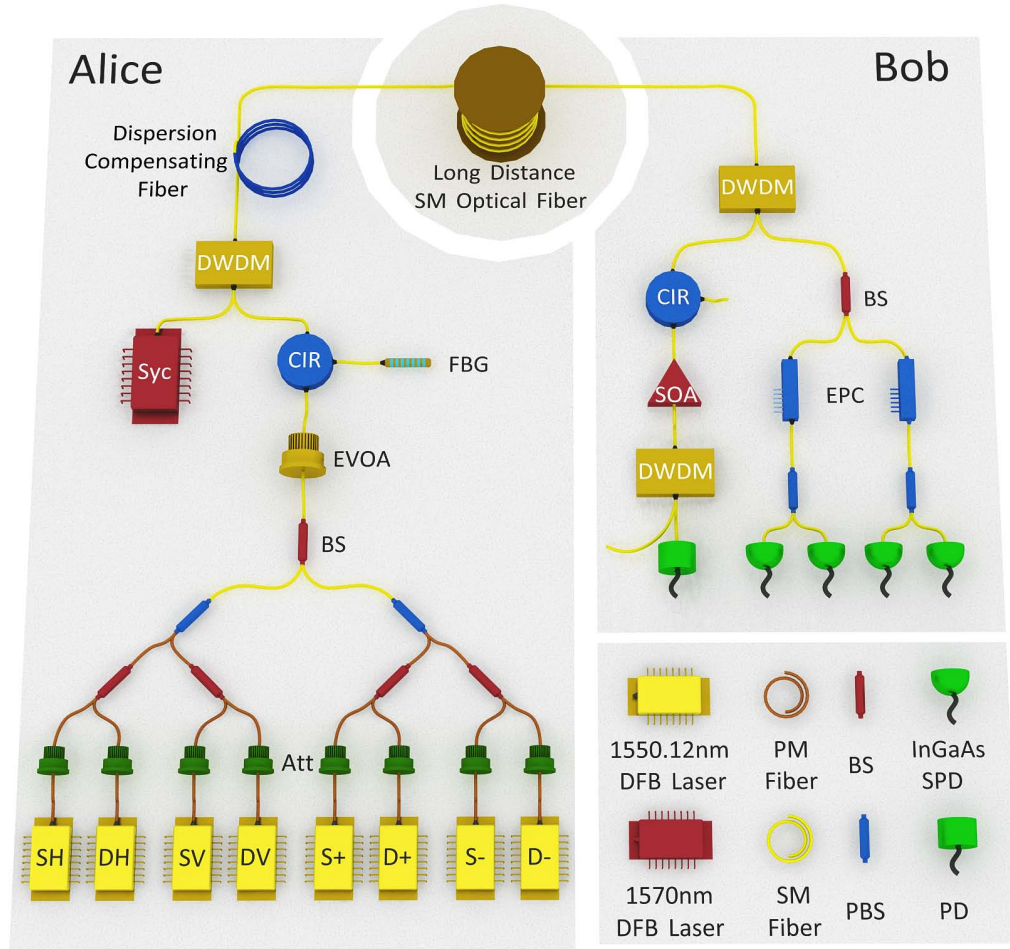


FIG. 1. Schematic layout of the experiment. DFB Laser: distributed feedback laser, Att: manual attenuator, PM: polarization maintaining, SM: single mode, BS: beam splitter, PBS: polarization beam splitter, EVOA: electrical variable optical attenuator, FBG: fiber Bragg grating, DCF: dispersion compensating fiber, DWDM: dense wavelength division multiplexer, SOA: semiconductor optical amplifier, EPC: electric polarization controllers, PD: photoelectric detector, APD: avalanche photodiode.

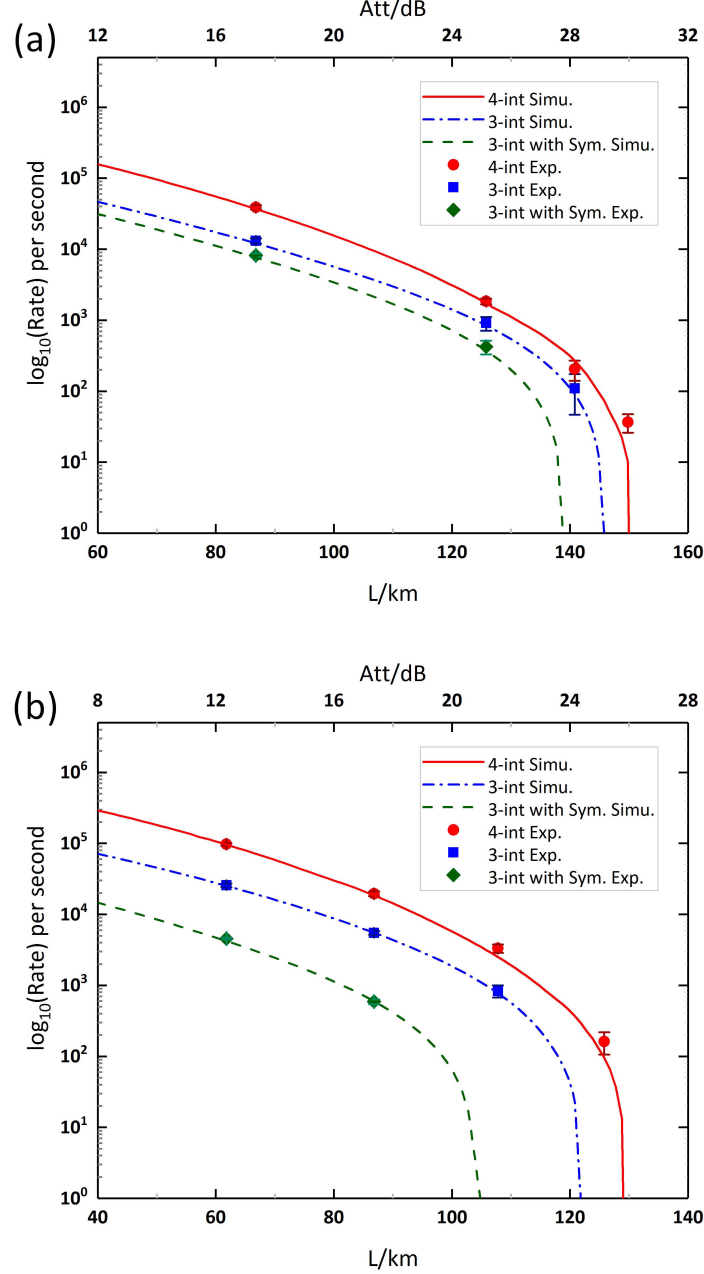


FIG. 2. Experimentally (symbols) and simulated (solid lines) secret key rates in bps versus the transmission distance in standard optical fiber. (a) the detector efficiency $\{\eta_Z, \eta_X\}$ is fixed at $\{10\%, 5\%\}$, while the experimental transmission distance are selected at 87, 126, 141 and 150 km. (b) the detector efficiency $\{\eta_Z, \eta_X\}$ is fixed at $\{10\%, 1\%\}$, while the experimental transmission distance are selected at 62, 87, 107 and 126 km. Blue squares, green diamonds and red circles, respectively, refers to (I) traditional 3-intensity protocol⁷ basis detector efficiencies symmetry, where Bob reduce higher detecotor efficiency to balance asymmetry $\eta_Z = \eta_X = 5\%$ or 1% ; (II) 3-intensity protocol with basis detector efficiencies asymmetry²¹, where $u_{X_2} = u_{Z_2}, u_{X_1} = u_{Z_1}, q_z = q_x, \eta_Z \neq \eta_X$; (III) 4-intensity protocol²¹, where $u_{X_2} \neq u_{Z_2}, u_{X_1} \neq u_{Z_1}, q_z \neq q_x, \eta_Z \neq \eta_X$. The experimental results are the average and variance (1 standard deviation, assuming Poissonian detection statistics) of the final key rate calculated by 30 experiments. The advantage of the 4-intensity protocol is clearly verified by the experimental results, especially in a large degree of basis detector efficiencies asymmetry. The results also confirm the excellent stability of three protocols used here.

TABLE I. List of parameters characterized for numerical optimization: detector dark count rate s_0 , detector After Pulses rate Ar , Detector dead time t_d in second, misalignment-error probability e_d , channel loss coefficient α in dB/km, error-correction efficiency f , security parameter ϵ , and the total number of laser pulses N

s_0	Ar	t_d	e_d	α	f	ϵ	N
2.50×10^{-7}	1%	5.00×10^{-7}	1.5%	0.2	1.14	10^{-10}	10^{10}

[!ht]

[!ht]

[!ht]

TABLE II. List of the main implementation parameters. Here, The notation u_{α_j} shown in the first column denotes the intensity of the coherent source α_j . p_{α_j} is the probability to use the source α_j in the protocol. p_0 is the probability to choose the vacuum source. q_X is the probability that Bob measures the received pulses in the X basis.

Parameters	62km(12.4dB)			87km(17.4dB)			107km(21.4dB)			126km(25.2dB)		
10%1%	3INT	(1%1%)	3INT	4INT	3INT	(1%1%)	3INT	4INT	3INT	4INT	3INT	4INT
u_{X_2}	0.134	0.145	0.145	0.418	0.515	0.501	0.714	0.499	0.671	0.560		
u_{Z_2}	0.134	0.145	0.145	0.470	0.515	0.501	0.453	0.499	0.449	0.429		
u_{X_1}	0.522	0.492	0.492	0.175	0.148	0.169	0.206	0.179	0.206	0.204		
u_{Z_1}	0.522	0.492	0.492	0.026	0.148	0.169	0.041	0.179	0.054	0.065		
p_{X_2}	0.406	0.418	0.418	0.030	0.327	0.365	0.032	0.272	0.040	0.034		
p_{Z_2}	0.406	0.418	0.418	0.754	0.327	0.365	0.693	0.272	0.577	0.288		
p_{X_1}	0.083	0.064	0.064	0.110	0.154	0.107	0.132	0.184	0.170	0.291		
p_{Z_1}	0.083	0.064	0.064	0.105	0.154	0.107	0.143	0.184	0.214	0.387		
p_0	0.022	0.036	0.036	NULL	0.038	0.055	NULL	0.088	NULL	NULL		
q_X	50%	50%	50%	15%	50%	50%	24%	50%	36%	55%		
10%5%	87km(17.4dB)			126km(25.2dB)			141km(28.2dB)			150km(30.0dB)		
u_{X_2}	0.524	0.521	0.521	0.473	0.513	0.513	0.451	0.512	0.621	0.572		
u_{Z_2}	0.524	0.521	0.521	0.516	0.513	0.513	0.445	0.512	0.459	0.523		
u_{X_1}	0.127	0.125	0.125	0.170	0.149	0.153	0.196	0.151	0.312	0.262		
u_{Z_1}	0.127	0.125	0.125	0.020	0.149	0.153	0.041	0.151	0.070	0.111		
p_{X_2}	0.421	0.428	0.428	0.019	0.294	0.331	0.037	0.200	0.055	0.098		
p_{Z_2}	0.421	0.428	0.428	0.772	0.294	0.331	0.531	0.200	0.338	0.175		
p_{X_1}	0.069	0.062	0.062	0.116	0.183	0.149	0.172	0.262	0.235	0.228		
p_{Z_1}	0.069	0.062	0.062	0.094	0.183	0.149	0.259	0.262	0.372	0.499		
p_0	0.020	0.020	0.020	NULL	0.045	0.041	NULL	0.076	NULL	NULL		
q_X	50%	50%	50%	13%	50%	50%	24%	50%	34%	50%		

TABLE III. List of the average and variance (1 standard deviation, assuming Poissonian detection statistics) of the total gains and error gains in the cases of $\{\eta_z = 10\%, \eta_x = 5\%\}$. The notation $\alpha_j\beta$ shown in the second column denotes the pulse from Alice source α_j and the basis β chosen by Bob, respectively.

Parameters	87km(17.4dB)				126km(25.2dB)				141km(28.2dB)				150km(30.0dB)			
	3INT(5%5%)	3INT	4INT	4INT	3INT(5%5%)	3INT	4INT	4INT	3INT	4INT	4INT	4INT	3INT	4INT	4INT	4INT
Total Gains	X_2X	551418.8 ± 13513.4	556153.6 ± 3713.5	5709.1 ± 177.0	64974.3 ± 499.2	73655.5 ± 1053.5	3698.1 ± 76.9	5335.4 ± 103.4	22636.7 ± 202.6	5335.4 ± 103.4	5335.4 ± 103.4	5335.4 ± 103.4	22636.7 ± 202.6	5335.4 ± 103.4	8441.0 ± 156.3	8441.0 ± 156.3
	X_1X	22246.4 ± 723.4	19234.5 ± 206.0	13826.9 ± 251.1	12376.7 ± 323.4	10122.4 ± 425.9	7499.0 ± 302.5	11369.8 ± 94.4	9422.2 ± 130.1	11369.8 ± 94.4	11369.8 ± 94.4	11369.8 ± 94.4	9422.2 ± 130.1	11369.8 ± 94.4	9416.2 ± 94.4	9416.2 ± 94.4
	X_0X	145.6 ± 18.8	143.6 ± 10.8	NUL	144.2 ± 12.9	130.7 ± 14.3	NUL	210.2 ± 16.5	210.2 ± 16.5	NUL	NUL	NUL	210.2 ± 16.5	NUL	NUL	NUL
	Z_2Z	532257.2 ± 13606.8	1072606.3 ± 6749.1	3340950.6 ± 27645.2	63247.3 ± 970.7	143018.1 ± 3543.1	302314.4 ± 2091.8	86861.5 ± 1534.9	43933.5 ± 613.3	86861.5 ± 1534.9	86861.5 ± 1534.9	86861.5 ± 1534.9	43933.5 ± 613.3	86861.5 ± 1534.9	25800.8 ± 285.3	25800.8 ± 285.3
	Z_1Z	22075.4 ± 648.5	38122.8 ± 348.8	18908.5 ± 248.9	12376.7 ± 177.4	19893.0 ± 314.7	15815.0 ± 382.9	16306.8 ± 277.3	18067.7 ± 379.3	16306.8 ± 277.3	16306.8 ± 277.3	16306.8 ± 277.3	18067.7 ± 379.3	16306.8 ± 277.3	17446.6 ± 218.3	17446.6 ± 218.3
	Z_0Z	144.3 ± 17.5	264.4 ± 19.3	NUL	140.1 ± 12.5	155.9 ± 14.9	NUL	212.3 ± 17.2	212.3 ± 17.2	NUL	NUL	NUL	212.3 ± 17.2	NUL	NUL	NUL
	X_2Z	547810.9 ± 12536.7	1068918.4 ± 9105.1	74118.7 ± 835.2	65447.0 ± 519.5	145119.9 ± 1851.1	21745.1 ± 271.7	19220.3 ± 293.2	44756.9 ± 736.4	19220.3 ± 293.2	19220.3 ± 293.2	19220.3 ± 293.2	44756.9 ± 736.4	19220.3 ± 293.2	15890.5 ± 164.8	15890.5 ± 164.8
	X_1Z	21825.1 ± 708.7	38409.7 ± 298.8	168526.6 ± 3115.7	12051.5 ± 301.1	19636.4 ± 585.8	43211.6 ± 1442.8	39677.8 ± 683.9	17560.9 ± 336.7	39677.8 ± 683.9	39677.8 ± 683.9	39677.8 ± 683.9	17560.9 ± 336.7	39677.8 ± 683.9	16696.5 ± 252.0	16696.5 ± 252.0
	X_0Z	144.8 ± 16.4	254.9 ± 16.8	NUL	145.2 ± 14.0	154.7 ± 15.2	NUL	207.6 ± 14.9	207.6 ± 14.9	NUL	NUL	NUL	207.6 ± 14.9	NUL	NUL	NUL
	Z_2X	539397.7 ± 14626.5	538231.6 ± 4594.5	264307.1 ± 3417.4	64809.0 ± 926.4	71796.5 ± 2782.3	50918.5 ± 515.7	24155.9 ± 424.6	22170.3 ± 274.8	24155.9 ± 424.6	24155.9 ± 424.6	24155.9 ± 424.6	22170.3 ± 274.8	24155.9 ± 424.6	13267.3 ± 218.8	13267.3 ± 218.8
	Z_1X	22203.6 ± 538.0	19728.7 ± 247.8	1843.7 ± 49.6	12401.1 ± 163.2	10292.6 ± 236.7	3453.1 ± 73.3	5520.6 ± 97.3	9551.0 ± 126.3	5520.6 ± 97.3	5520.6 ± 97.3	5520.6 ± 97.3	9551.0 ± 126.3	5520.6 ± 97.3	10023.2 ± 100.0	10023.2 ± 100.0
	Z_0X	144.5 ± 17.4	142.5 ± 14.1	NUL	138.1 ± 11.5	131.4 ± 13.9	NUL	211.5 ± 17.8	211.5 ± 17.8	NUL	NUL	NUL	211.5 ± 17.8	NUL	NUL	NUL
Error Gains	X_2X	9199.7 ± 2236.8	8747.8 ± 784.3	143.9 ± 14.4	1664.3 ± 147.5	1840.7 ± 312.9	154.9 ± 16.2	340.3 ± 27.3	853.1 ± 148.2	216.6 ± 30.8	216.6 ± 30.8	216.6 ± 30.8	853.1 ± 148.2	216.6 ± 30.8	340.3 ± 27.3	340.3 ± 27.3
	X_1X	741.8 ± 129.3	635.9 ± 36.2	600.8 ± 30.1	706.8 ± 32.1	584.2 ± 62.7	554.0 ± 38.6	634.1 ± 29.1	841.0 ± 92.5	748.8 ± 66.2	748.8 ± 66.2	748.8 ± 66.2	841.0 ± 92.5	748.8 ± 66.2	634.1 ± 29.1	634.1 ± 29.1
	X_0X	73.4 ± 9.2	72.9 ± 8.2	NUL	74.1 ± 9.8	64.9 ± 10.3	NUL	106.5 ± 9.6	106.5 ± 9.6	NUL	NUL	NUL	106.5 ± 9.6	NUL	NUL	NUL
	Z_2Z	12363.2 ± 2150.4	22007.5 ± 3341.7	62990.5 ± 4278.1	1925.5 ± 289.2	3644.1 ± 263.3	6533.8 ± 640.6	797.1 ± 62.7	1171.3 ± 80.9	2410.9 ± 204.2	2410.9 ± 204.2	2410.9 ± 204.2	1171.3 ± 80.9	2410.9 ± 204.2	797.1 ± 62.7	797.1 ± 62.7
	Z_1Z	864.0 ± 107.4	1361.4 ± 111.4	1999.8 ± 96.5	747.4 ± 56.6	886.1 ± 43.8	1357.3 ± 75.9	1533.3 ± 57.3	974.3 ± 48.4	1379.0 ± 36.7	1379.0 ± 36.7	1379.0 ± 36.7	974.3 ± 48.4	1379.0 ± 36.7	1533.3 ± 57.3	1533.3 ± 57.3
	Z_0Z	71.8 ± 9.5	133.1 ± 12.6	NUL	70.7 ± 9.6	79.7 ± 10.7	NUL	106.9 ± 12.1	106.9 ± 12.1	NUL	NUL	NUL	106.9 ± 12.1	NUL	NUL	NUL
	R	1.32E-05 $\pm 8.07E-07$	2.12E-05 $\pm 1.77E-06$	6.30E-05 $\pm 4.02E-06$	6.81E-07 $\pm 1.50E-07$	1.48E-06 $\pm 3.25E-07$	2.98E-06 $\pm 2.77E-07$	5.93E-08 $\pm 1.71E-08$	1.78E-07 $\pm 1.03E-07$	3.30E-07 $\pm 1.04E-07$	3.30E-07 $\pm 1.04E-07$	3.30E-07 $\pm 1.04E-07$	1.78E-07 $\pm 1.03E-07$	3.30E-07 $\pm 1.04E-07$	5.93E-08 $\pm 1.71E-08$	5.93E-08 $\pm 1.71E-08$

TABLE IV. List of the average and variance (1 standard deviation, assuming Poissonian detection statistics) of the total gains and error gains in the cases of $\{\eta_z = 10\%, \eta_x = 1\%\}$. The notation $\alpha_j\beta$ shown in the second column denotes the pulse from Alice source α_j and the basis β chosen by Bob, respectively.

Parameters 10%1%	62km(12.4dB)				87km(17.4dB)				107km(21.4dB)				126km(25.2dB)			
	3INT(1%1%)	3INT	4INT	4INT	3INT(1%1%)	3INT	4INT	4INT	3INT	4INT	4INT	4INT	3INT	4INT	4INT	4INT
Total Gains	X_2X	330399.5 ± 6573.9	312310.7 ± 5027.8	6007.4 ± 134.4	83854.6 ± 1022.9	93979.9 ± 1661.1	5873.1 ± 160.5	28473.8 ± 734.5	4037.7 ± 81.4	1972.3 ± 51.8						
	X_1X	18234.3 ± 238.5	15305.9 ± 174.6	9738.6 ± 146.1	11901.2 ± 307.5	9710.8 ± 156.2	7366.3 ± 99.2	7557.3 ± 201.2	5715.3 ± 149.5	6658.3 ± 151.7						
	X_0X	120.1 ± 11.8	201.9 ± 15.5	NULL	126.6 ± 15.1	188.4 ± 16.5	NULL	236.3 ± 13.8	NULL	NULL						
	Z_2Z	341589.9 ± 5789.6	2885578.7 ± 26291.5	8152239.7 ± 153051.7	86854.9 ± 1458.3	893901.8 ± 12110.0	2308003.1 ± 41297.7	271688.1 ± 3812.4	647788.3 ± 14340.1	93277.2 ± 1145.7						
	Z_1Z	18789.9 ± 235.3	133707.8 ± 435.9	70249.0 ± 1136.4	12342.7 ± 250.8	88989.3 ± 1698.2	46308.4 ± 270.7	65140.2 ± 995.3	31450.7 ± 607.3	21229.4 ± 281.8						
	Z_0Z	119.4 ± 13.1	1027.6 ± 48.4	NULL	127.0 ± 13.7	589.6 ± 35.6	NULL	456.8 ± 18.6	NULL	NULL						
	X_2Z	347785.7 ± 1595.7	2993230.8 ± 4815.9	291752.5 ± 2585.1	86737.4 ± 1638.3	891406.4 ± 8560.7	169139.3 ± 2999.7	270912.9 ± 2959.6	67148.5 ± 1593.0	14662.1 ± 221.0						
	X_1Z	18474.7 ± 401.0	131317.7 ± 1233.1	449001.8 ± 7198.0	12382.3 ± 307.3	88134.9 ± 1180.9	195019.6 ± 2437.9	65305.2 ± 765.7	85263.0 ± 2731.9	44475.4 ± 1011.4						
	X_0Z	121.7 ± 10.9	1015.8 ± 45.3	NULL	124.5 ± 12.0	591.6 ± 29.7	NULL	454.7 ± 23.5	NULL	NULL						
	Z_2X	339096.4 ± 3402.7	321268.0 ± 2897.1	173910.1 ± 1725.4	82948.8 ± 528.8	91943.3 ± 1347.1	80238.4 ± 1168.3	27745.8 ± 690.8	39802.4 ± 771.1	12868.8 ± 292.3						
Error Gains	Z_1X	18127.1 ± 241.5	14025.7 ± 268.3	1913.4 ± 52.7	11864.5 ± 185.8	9535.2 ± 158.6	2174.9 ± 46.4	7327.3 ± 182.7	2696.9 ± 71.8	4157.0 ± 95.1						
	Z_0X	121.1 ± 13.2	199.8 ± 14.6	NULL	126.7 ± 19.0	185.3 ± 13.1	NULL	239.2 ± 16.5	NULL	NULL						
	X_2X	6102.5 ± 826.0	6646.1 ± 585.4	173.2 ± 25.1	2182.3 ± 265.5	2680.2 ± 410.9	159.6 ± 33.7	1050.0 ± 116.7	135.6 ± 16.4	92.9 ± 10.1						
	X_1X	676.2 ± 57.2	549.3 ± 30.3	471.9 ± 43.5	674.9 ± 84.0	502.4 ± 47.6	441.9 ± 34.9	572.0 ± 36.5	465.1 ± 36.9	727.7 ± 61.4						
	X_0X	58.7 ± 7.4	102.5 ± 11.7	NULL	63.1 ± 9.8	93.8 ± 10.7	NULL	115.9 ± 9.7	NULL	NULL						
	Z_2Z	7969.1 ± 890.3	55921.2 ± 5978.7	155437.3 ± 15126.6	2284.4 ± 169.8	15283.9 ± 837.0	44795.7 ± 1056.5	5387.8 ± 518.6	13137.3 ± 693.9	2241.6 ± 132.3						
	Z_1Z	748.5 ± 44.7	3687.2 ± 315.7	5446.5 ± 374.7	677.6 ± 45.1	2290.0 ± 76.8	2785.2 ± 131.7	1930.9 ± 126.5	1843.4 ± 46.0	1588.0 ± 71.8						
	Z_0Z	59.8 ± 8.3	515.9 ± 24.8	NULL	63.6 ± 8.6	294.0 ± 25.4	NULL	229.2 ± 19.1	NULL	NULL						
	R	7.36E-06 $\pm 2.67E-07$	4.15E-05 $\pm 2.34E-06$	1.57E-04 $\pm 7.26E-06$	9.53E-07 $\pm 7.58E-08$	8.90E-06 $\pm 5.43E-07$	3.16E-05 $\pm 2.42E-06$	1.35E-06 $\pm 2.60E-07$	5.36E-06 $\pm 7.26E-07$	2.62E-07 $\pm 9.03E-08$						